*Edvard Bjelajac[1,a], Andrej Skumavc[2], Tomaž Vuherer [3,b],Nenad Gubeljak [3,c], Damjan Klobčar [4,d], Gorazd Lojen [3,e]*

# COMPARISON OF WELDS MADE WITH A LASER WELDING MACHINE UNDER DIFFERENT SHIELDING GASES

# POREĐENJE ZAVARENIH SPOJEVA DOBIJENIH LASERSKIM POSTUPKOM ZAVARIVANJA U ATMOSFERI RAZLIČITIH ZAŠTITNIH GASOVA

**Original scientific paper / Originalni naučni rad**

**Paper received / Rad primljen:**

*July 2026.*

**Paper accepted / Rad prihvaćen:**

*August 2026.*

**Author's address / Adresa autora:**

*[1] Messer Slovenija d.o.o., Ruše, Republic of Slovenia*

*[2] SIJ Acroni, Jesenice, Republic of Slovenia*

*[3] Faculty of Mechanical Engineering, University of Maribor, Maribor, Republic of Slovenia*

*[4] Faculty of Mechanical Engineering, University of Ljubljana, Ljubljana, Republic of Slovenia*

**Email / ORCID ID:**

*[a] edvard.bjelajac@messergroup.com /*

*/ [b] 0000-0002-1866-8266*

*/ [c] 0000-0002-3276-8431*

*/ [d] 0000-0002-6130-0328*

/ [e] 0000-0002-9757-5710

**Keywords:** laser welding, shielding gases, tensile properties, hardness

**Ključne reči:** lasersko zavarivanje, zaštitni gasovi, svojstva na zatezanje, tvrdoća

## Abstract

Welding of S235 pickled structural steel sheets was performed in a Trumpf TruLaser 5000 laser cell to determine the effect of the protective atmosphere on welding parameters, microstructure, and mechanical properties of the welded joint. Three series of samples were welded. The first two were produced in a protective atmosphere of argon and nitrogen. The third series of samples was processed without shielding gas. Metallographic cross-sections were prepared, the microstructure was examined, geometry of welded joints was analyzed, tensile tests and hardness measurements were done.

## Rezime

Zavarivanje konstrukcionog čelika S235 u dekapiranom stanju urađeno je na laserskoj ćeliji Trumpf TruLaser 5000 kako bi se utvrdio utjicaj zaštitne atmosfere na parametre zavarivanja, mikrostrukturu i mehaničke osobine zavarenog spoja. Zavarene su tri serije uzoraka. Prve dvije serije uzoraka zavarene su u zaštitnoj atmosferi argona i azota. Treća serija uzoraka obrađena je bez upotrebe zaštitnog gasa. Pripremljeni su metalografski uzorci, ispitana je mikrostruktura i geometrija zavarenih spojeva. Na kraju su bila sprovedena ispitivanja na zatezanje i mjerenje tvrdoće.

*The paper was published in its original form in the Proceedings of the 1st Conference with international participation "Technology of Joining Materials" held in Bečići, Montenegro from May 14 to 16, 2026.*

## 1. Introduction

MAG welding with an active shielding gas or the MIG process using inert gas is the most commonly used arc process for joining metal materials in industrial practice. MAG processes are highly productive, and their productivity can be further increased by optimizing the composition of the shielding gas mixture. The advantages of the MAG process also include easy inspection of the welded joint, the possibility of precise observation of the weld pool, the possibility of combining a wide range of materials, good mechanical properties of joints, and easy mechanization and robotization of the welding process [1 - 3].

As the thickness of the base material decreases, technological problems arise in practice during MIG/MAG processes. These are mainly related to high heat input, resulting in internal stresses and deformations in the product [4, 5]. In addition, spatter often occurs, which reduces the aesthetic appearance of the weld and increases the amount of work required after welding [6].

Laser welding, with or without filler material, has recently become established for welding thin sheets of non-alloy structural steels, high-alloy steels, and non-ferrous metals. It should be noted that the laser heat source differs significantly from the classic MAG source. The metallurgical processes that take place during laser welding differ from those in arc welding methods. Consequently, the properties of laser-welded joints also differ from those achieved using conventional technologies [7 - 9].

One of the modern solutions in the field of laser welding are hand-held laser welding devices, which have been developing rapidly in recent years. They operate with a laser beam generated by power sources mostly between 1 kW and 3 kW. Currently, sources with a power of 2 kW are most commonly used in industrial environments [4, 10].

The choice of shielding gases depends on the base material. In MAG arc welding, argon-based shielding gases containing active components such as carbon dioxide, oxygen, nitrogen, and hydrogen, as well as the inert gas helium, are commonly used. The active components react with the base material and affect the mechanical properties in the weld area [11].

In laser welding, in addition to inert gas argon, nitrogen is also very often used as a basic shielding gas, for welding of unalloyed structural steels, high-alloy stainless steels, as well as non-ferrous metals [11].

The effect of nitrogen on steel during arc and laser welding was investigated by Kokawa [11]. He found that the absorption/desorption of nitrogen by molten metal is influenced by many factors, including the chemical composition of the base material, the partial pressure of the gas, the equilibrium solubility of nitrogen, reaction rate, melt pool configuration, and its change over time. By defining these factors, it is possible to understand the absorption/desorption in the molten metal and make a quantitative prediction of the nitrogen content. It is assumed that the phenomenon can be understood by using empirical data on the chemical composition of materials and the welding process, taking into account only a few predominant factors. It should be noted that absorption/desorption of nitrogen is closely related to formation of porosity [11].

The aim of this research was to produce butt welds on the base material S235 by laser welding without a filler material. The laser beam power was the same for all samples, while the welding speed varied depending on the type of protective atmosphere. To determine the effect of shielding gases on microstructure, geometry, and mechanical properties of the welded joint, three groups of experiments were conducted: welding with argon, welding with nitrogen, and the third, welding in air, without any shielding gas. Microstructures of the welds were examined, geometries of weld metal and HAZ cross-sections analyzed, and tensile strengths and hardness were determined.

## 2. Materials and methods

### *2.1. Material*

For this study, 6 mm-thick structural steel S235JR+N, in accordance with EN 10025-2, was used as the base material. The chemical composition of the steel is presented in Table 1. According to EN 10204 3.1 ATEST of the steel, the yield stress of the steel ($R_{eH}$) is 322 MPa, the ultimate tensile strength ($R_m$) is 437 MPa, and the elongation of the steel ($A_5$) is 34 %.

***Table 1.*** *Chemical composition of the base material S235 JR+M (wt.%).*

***Tabela 1.*** *Hemijski sastav osnovnog materijala S235JR+M (u mas.%).*

| C | Mn | Si | P | S | Cr | Ni | Cu | Al | N | Fe |
|---|---|---|---|---|---|---|---|---|---|---|
| 0.14 | 0.51 | 0.01 | 0.011 | 0.006 | 0.03 | 0.01 | 0.01 | 0.034 | 0.004 | rest |

*2.2. Welding*

Welding was carried out in a laser robotic cell TruLaser Weld 5000. A Trumpf fiber laser TruLaser 5000 was used in combination with a Kuka's six-axis high-precision industrial robot KR 30 HA, The robot payload capacity is 30 kg and its reach is 2033 mm. The robotic cell is shown in Figure 1.



***Figure 1.*** *The laser robotic cell TruLaser Weld 5000.*

***Slika 1.*** *Robotska ćelija za lasersko zavarivanje TruLaser Weld 5000.*

The specimen designations and welding parameters are presented in Table 2. During the welding process, the laser power was kept constant at 3000 W. The focal position of the laser beam was varied, with the focal point located at different depths below the surface of the weldment ($f$ = – 2 mm to – 4 mm), and the welding speed was also adjusted ($v$ = 5 mm/s to 10 mm/s). Consequently, the linear heat input varied in the range of 0.3 kJ/mm to 0.6 kJ/mm. Welding was performed either with or without shielding gas. When applied, the shielding gas was either argon or nitrogen, each at a flow rate of 20 l/min. The third laser welding was performed without any shielding gas.

***Table 2.*** *Designation of the specimens and parameter of laser welding.*

***Tabela 2.*** *Oznake uzoraka i parametri laserskog zavarivanja.*

| Specimen mark | **LA-1** | **LA-2** | **LA-3** | **LA-4** |
|---|---|---|---|---|
| $P$ = 3000 W<br>Shielding gas Ar | $f$ = -3 mm<br>$v$ = 5 mm/s<br>$Q$ = 0.6 KJ/mm | $f$ = -3 mm<br>$v$ = 5 mm/s<br>$Q$ = 0.6 KJ/mm | $f$ = -4 mm<br>$v$ = 5 mm/s<br>$Q$ = 0.6 KJ/mm | $f$ = -2 mm<br>$v$ = 5 mm/s<br>$Q$ = 0.6 KJ/mm |
| Specimen mark | **LN-1** | **LN-2** | **LN-3** | |
| $P$ = 3000 W<br>Shielding gas $N_2$ | $f$ = -3 mm<br>$v$ = 5 mm/s<br>$Q$ = 0.6 KJ/mm | $f$ = -3 mm<br>$v$ = 7 mm/s<br>$Q$ = 0.43 KJ/mm | $f$ = -3 mm<br>$v$ = 8 mm/s<br>$Q$ = 0.375 KJ/mm | – |
| Specimen mark | **LB-1** | **LB-2** | **LB-3** | |
| $P$ = 3000 W<br>Without gas | $f$ = -3 mm<br>$v$ = 5 mm/s<br>$Q$ = 0.6 KJ/mm | $f$ = -3 mm<br>$v$ = 8 mm/s<br>$Q$ = 0.375 KJ/mm | $f$ = -3 mm<br>$v$ = 10 mm/s<br>$Q$ = 0.3 KJ/mm | – |

*2.3. Macro section and weld geometry measurement*

We prepared macro-polished sections from all welded samples. Grinding was performed using wet-grinding papers with various grain sizes ranging from P100 to P1000. Final polishing was performed using 0.5 μm $Al_2O_3$. Finally, the macro-polished surfaces were etched with 3 % nitric acid (3 % nital) for 15 seconds.

All macro samples were photographed and analyzed using a Leica Wild M10 light microscope. Particular attention was paid to the geometry of the welded joint, where the weld width (WW), root width (RW) and penetration depth (P) of the weld were measured (Figure 2). The face reinforcement (FR) and root reinforcement (RR) were also measured, as well as concavities, i.e. the weld face negative reinforcement (– FR) and negative root reinforcement (– RR) of the weld. The weld cross-sectional area was also measured.

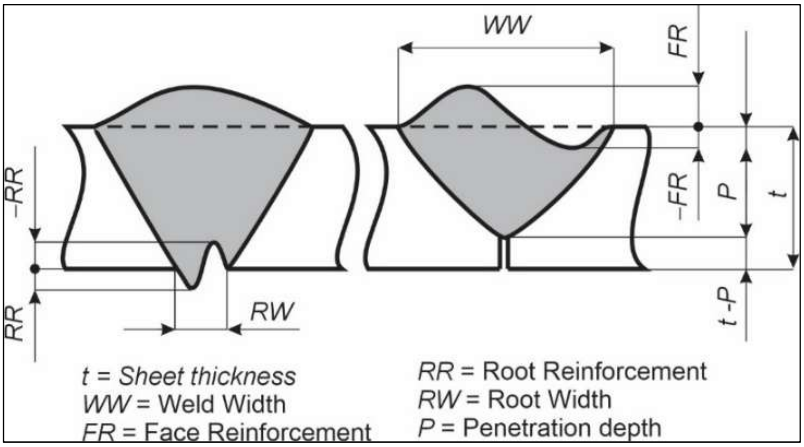



***Figure 2.*** *Measured weld geometry.*

***Slika 2.*** *Izmerena geometrija zavarenog spoja.*

*2.3. Mechanical properties*

Based on the best-measured weld geometry on the macro-grinds and welds free of any defects, we selected one weld from each group as a reference weld for further analysis.

The microstructure of the reference welds was analyzed, and Vickers hardness was measured using a 10 kg load. Hardness was measured in the root and root-face regions of the weld, as shown in Figure 3. At least three measurements were taken in each area (BM, HAZ, WM, HAZ, BM).

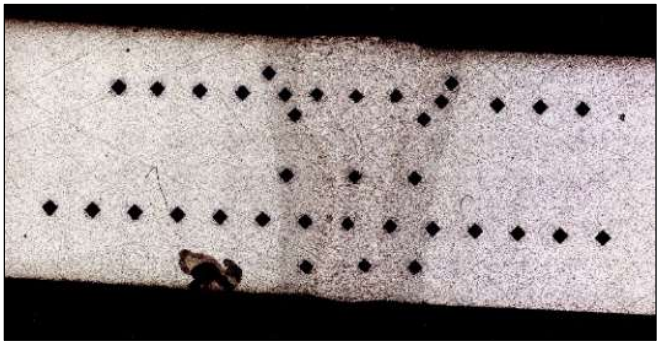


***Figure 3.*** *Vickers hardness measurements in the crown and root of the weld.*

***Slika 3.*** *Merenje tvrdoće po Vikersu u licu i korenu zavarenog spoja.*

Tensile tests were performed on the base materials of selected welded joints in accordance with EN ISO 6892-1[12], and tensile tests on the welded joints were performed in accordance with EN ISO 5178[13]. Two tensile tests were performed on each part using a flat tensile test specimen (10 mm wide and 6 mm thick). A total of 12 tensile tests were performed, 6 on the base metal and 6 on the welds.

## 3. Results and discussion

### *3.1. Macrosection*

Macrographs were prepared for all 10 welds, as shown in Figure 4. The figures include the focal length of the laser beam below the weld surface and the linear heat input. The first column shows macro-sections of laser welding where argon 4.6 was used as the shielding gas during welding. These welds are labelled LA-1 through LA-4. As can be seen, porosity is present in the weld, which we attempted to eliminate by adjusting the focal depth of the laser beam below the weld surface. We succeeded to some extent by increasing or decreasing the focal depth, but we achieved complete penetration only by reducing the focal depth to – 2 mm. This weld was then further analysed.

The middle column in Figure 4 shows samples of welds made in a nitrogen 5.0 shielding gas, labelled LN-1 through LN-3. In the first two samples, we achieved complete fusion, but not in the third, as the heat input was too low ($Q$ = 0.375 kJ/mm). In the first case, at the maximum heat input ($Q$ = 0.6 kJ/mm), occasional drips appeared at the root along the weld, so we selected weld LN-2 for further analysis.

The last column in Figure 4 shows macrographs of welds where no shielding gas was used during welding, labelled LB-1 through LB-3. In the case of the highest heat input LB-1 (Q = 0.6 kJ/mm), a lack of material appeared at the crown and sagging at the root. In the case of the lowest heat input at LN-3 (Q = 0.3 kJ/mm), we were unable to fully penetrate the weld, and an increased crown height of the weld also appeared. For this reason, we selected sample LB-2 for further analysis, where we were able to fully penetrate the weld without material loss at the crown and without an increased undercut at the root of the weld.

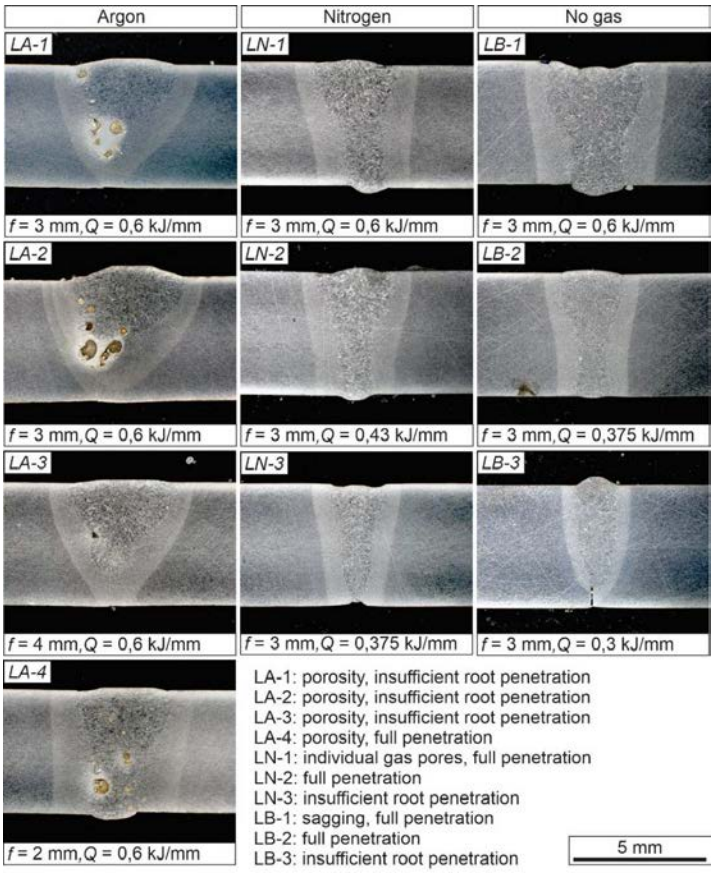



***Figure 4.*** *Macro-scale examination of laser-welded joints with different welding parameters and various shielding atmospheres.*

***Slika 4.*** *Makroskopsko ispitivanje laserski zavarenih spojeva izrađenih pri različitim parametrima zavarivanja i u različitim zaštitnim atmosferama.*

### *3.2. Analysis of weld geometry measurements results*

The geometry of the welded joints on selected LA-4, LN-2, and LB-2 macro sections was analyzed in detail in accordance with the designations shown in Figure 5. The results of the measurements of the weld geometries and the surfaces of the weld sections are presented in Table 3 and Table 4.

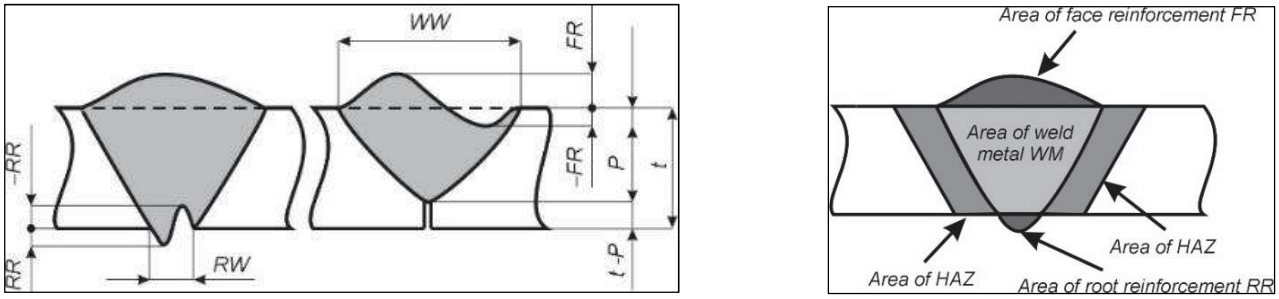



***Figure 5.*** *Weld geometry; a) dimensions; b) surfaces*

***Slika 5.*** *Geometrija zavarenog spoja: a) dimenzije; b) površine*

***Table 3.*** *Analysis of dimensions of welded joints in accordance with Figure 5a.*

***Tabela 3.*** *Analiza dimenzija zavarenih spojeva u skladu sa Slikom 5a.*

| Specimen | LA-4 | LN-2 | LB-2 |
|---|---|---|---|
| Weld face width *WW* / mm | 4.67 | 3.91 | 2.70 |
| Face reinforcement *FR* / mm | 0.12 | 0.21 | 0.17 |
| Root width *RW* / mm | 2.33 | 1.78 | 1.63 |
| Root reinforcement *RR* / mm | 0.37 | 0.26 | 0.01 |
| Max HAZ width / mm | 2.08 | 1.39 | 1.1 |
| Min. HAZ width / mm | 1.08 | 0.79 | 0.78 |
| Max. weld width of affected area / mm | 7.16 | 5.49 | 4.80 |

***Table 4.*** *Analysis of the areas of welded joints according to Figure 5b.*

***Tabela 4.*** *Analiza površina zavarenih spojeva u skladu sa slikom 5b.*

| Specimen | LA-4 | LB-2 | LN-2 |
|---|---|---|---|
| Face reinforcement *FR* / mm$^2$ | 3.46 | 0.38 | 0.28 |
| Root reinforcement *RR* / mm$^2$ | 5.21 | 0.07 | 0.29 |
| Weld metal area WM/ mm$^2$ | 20.46 | 12.66 | 15.03 |
| HAZ area / mm$^2$ | 19.56 | 12.07 | 13.21 |
| Weld metal + HAZ mm$^2$ | 41.00 | 24.73 | 28.24 |
| Porosity | Yes | No | No |

The measured dimensions and surface areas show that the widest weld and the weld with the largest surface area is achieved when welding with argon; however, there may be a problem with insufficient penetration, as can be seen from the cross-sectional images. Porosity also occasionally occurs here due to trapped gases during welding and insufficient degassing of the weld pool. A wider heat-affected zone (HAZ) and a larger HAZ surface area are also observed in argon welding.

When comparing welding with nitrogen and without shielding gas, we observed that welds of the same shape were achieved even when the heat inputs differed slightly. In the case of welding with nitrogen, an approximately 13 % higher heat input was necessary for the same weld area. This can be attributed to the difference in thermal conductivity between the individual gases. In both cases, however, it can be observed that there is no porosity in the weld. When the heat input is the same ($Q$ = 0.6 kJ/mm, Figure 4), we can observe a lack of material at the weld crown in the weld made without shielding gas and an increased sagging at the root of the weld. The root is also wider.

### *3.3. Hardness measurement results*

Figures 6 through 8 show the results of Vickers hardness measurements using a 10 kg load in individual sections of the weld. In all three cases, the highest hardness is found in the weld. In the heat-affected zone, however, the hardness gradually decreases toward the base material as the distance from the weld increases. The lowest hardness was measured in the base material.

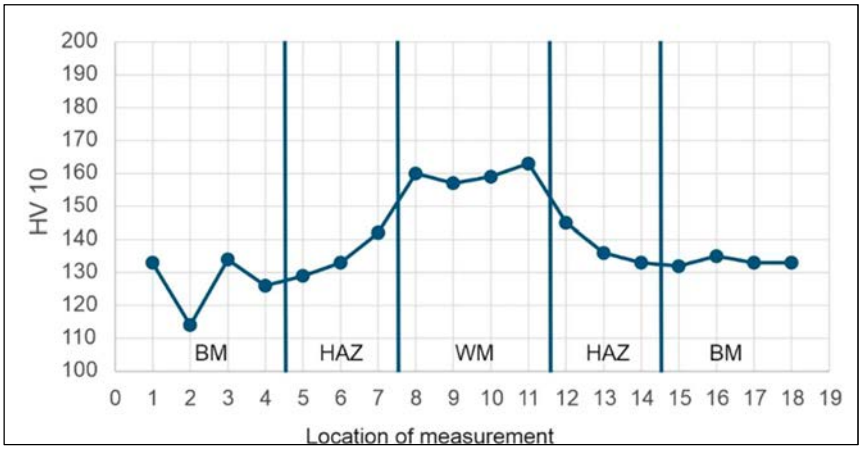



***Figure 6.*** *Hardness measurements on a laser-welded joint in an argon atmosphere – LA-4.*

***Slika 6.*** *Rezultati merenja tvrdoće laserski zavarenog spoja izrađenog u atmosferi argona – LA-4.*

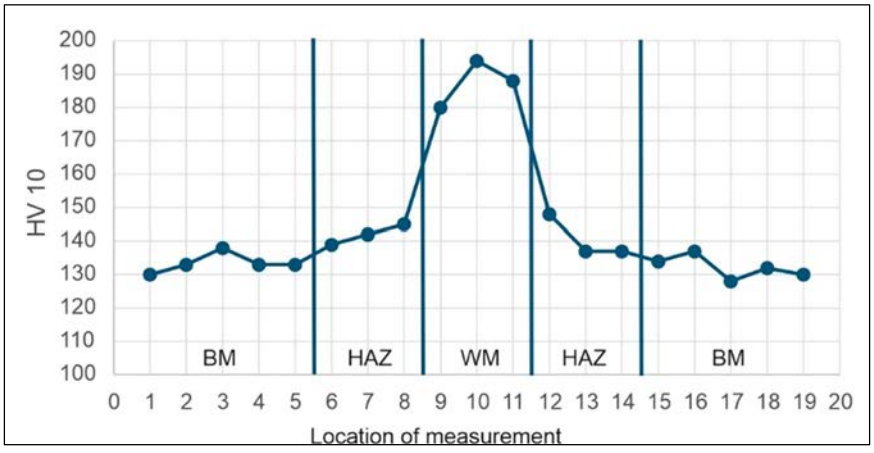



***Figure 7.*** *Hardness measurements on a laser-welded joint in a nitrogen atmosphere – LN-2.*

***Slika 7.*** *Rezultati merenja tvrdoće laserski zavarenog spoja izrađenog u atmosferi azota – LN-2.*

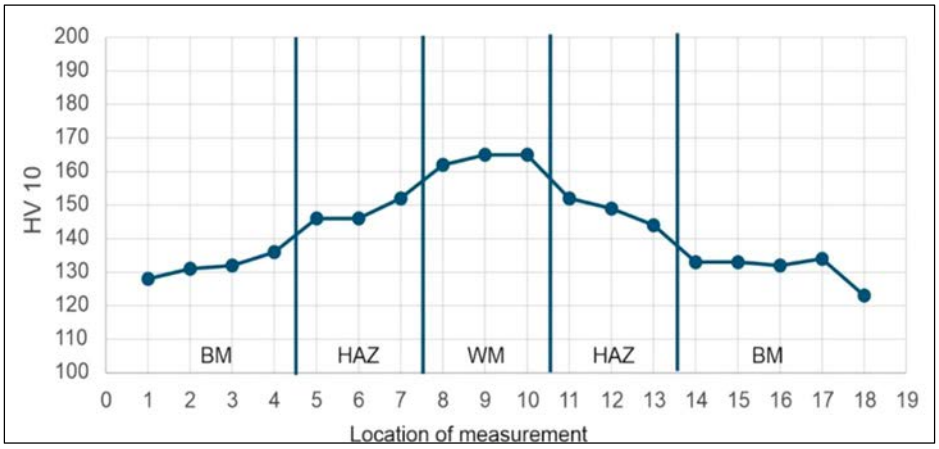



***Figure 8.*** *Hardness measurements on an unprotected laser weld – LB-2.*

***Slika 8.*** *Rezultati merenja tvrdoće laserski zavarenog spoja bez primene zaštitne atmosfere – LB-2.*

We measured the highest hardness in the weld on the LN-2 sample, which was welded in a nitrogen shielding gas, where heat input was minimal. Compared to the base material, the hardness increased by approximately 50% to about 195 HV10.

The lowest hardness in the welds was measured in samples welded with argon shielding gas. The increase in hardness relative to the base material was approximately 23% in the weld, reaching about 160 HV10.

We observed a similar result in welding without shielding gas, where the increase in hardness in the weld compared to the base material was approximately 28% to 169 HV10. This weld, however, was made with the lowest heat input ($Q$ = 0.375 kJ/mm) among the welds selected for analysis.

### *3.4. Results of tensile tests*

A total of 12 test specimens were tested - 6 welded specimens and 6 made solely of the base material, with four from each series, Figure 9, Figure 10, and Figure 11. All fractures occurred in the base material. In the specimens with a weld in the middle, the material failed in the middle between the clamping and the weld; in the specimens without a weld, the failure occurred near the middle of the tensile specimen.




***Figure 9.*** *Tensile test specimens LA-4, welded with argon and base metal: (a) before and (b) after the tensile test.*

***Slika 9.*** *Epruvete LA-4, zavarene u atmosferi argona, i epruvete od osnovnog materijala za ispitivanje zatezanjem: a) pre i b) nakon ispitivanja.*

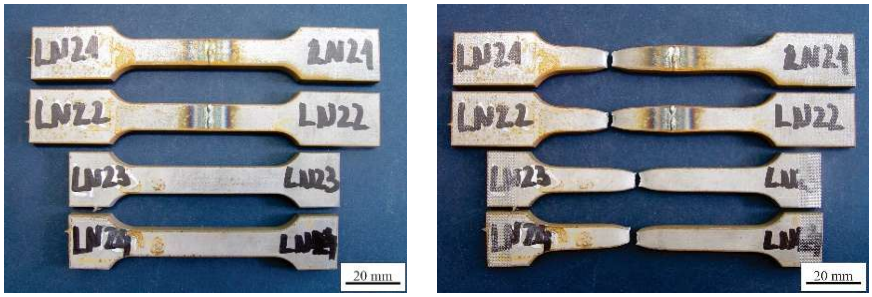



***Figure 10.*** *Tensile test specimens LN-2, welded with nitrogen and base metal: (a) before and (b) after the tensile test.*

***Slika 10.*** *Epruvete LN-2, zavarene u atmosferi azota, i epruvete od osnovnog materijala za ispitivanje zatezanjem: a) pre i b) nakon ispitivanja.*

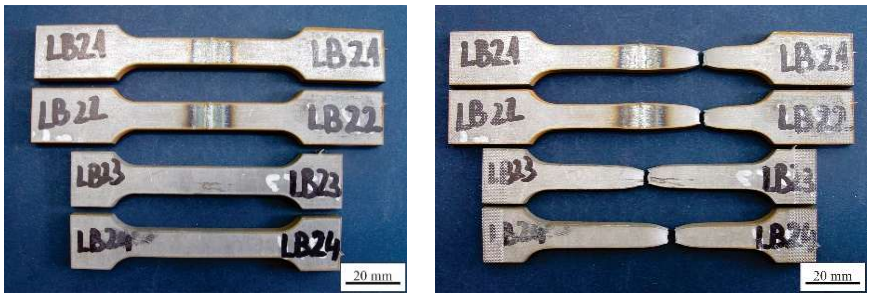



***Figure 11.*** *Tensile test specimens LB-2, welded without shielding gas and base metal: (a) before and (b) after the tensile test.*

***Slika 11.*** *Epruvete LB-2, zavarene bez primene zaštitnog gasa, i epruvete od osnovnog materijala za ispitivanje zatezanjem: a) pre i b) nakon ispitivanja.*

As can be seen, all welded samples fractured in the base material, and the stress-strain curves were very similar to those of the base material. For this reason, we present only one typical tensile test curve, shown in Figure 12.

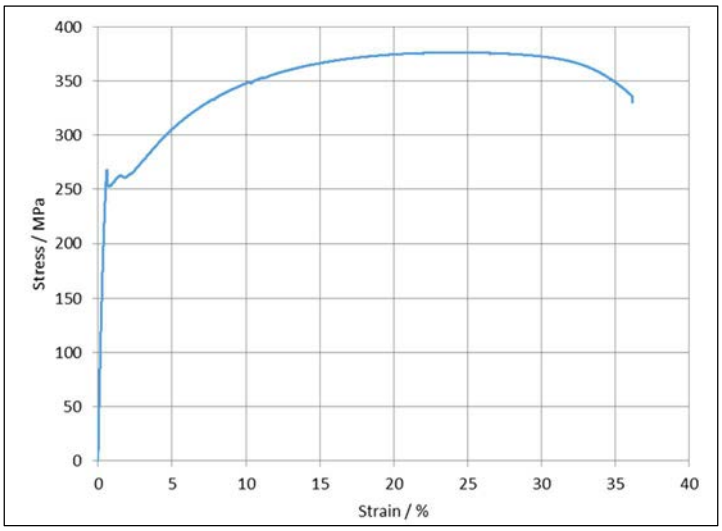



***Figure 12.*** *Strain-Stress diagram of the tensile test specimen LB-23.*

***Slika 12.*** *Dijagram napon–deformacija epruvete LB-23 ispitane zatezanjem.*

The results of the tensile tests are presented in Table 5, which shows the yield strength $R_{p0.2}$ or $R_{eH}$, the tensile strength $R_m$, the elongation $A$, and the reduction in area $Z$. All the breaks are in the BM, so the results are very similar.

***Table 5.*** *Results of tensile tests on welds and base material.*

***Tabela 5.*** *Rezultati ispitivanja zatezanjem zavarenih spojeva i osnovnog materijala.*

| Specimen ID | $R_{p0.2}$ / MPa | $R_{eH}$ / MPa | $R_m$ / MPa | *A* / % | *Z* / % |
|---|---|---|---|---|---|
| LB21 | 243 | – | 380 | 34 | 75 |
| LB22 | 229 | – | 378 | 34 | 68 |
| LB23 | 268 | 268 | 376 | 33 | 58 |
| LB24 | 260 | 261 | 374 | 35 | 47 |
| LA41 | 248 | – | 383 | 33 | 69 |
| LA42 | 241 | – | 382 | 32 | 63 |
| LA43 | 263 | 263 | 374 | 34 | 43 |
| LA44 | 264 | 267 | 376 | 33 | 71 |
| LN21 | 251 | – | 381 | 33 | 65 |
| LN22 | 240 | – | 382 | 34 | 70 |
| LN23 | 257 | 262 | 376 | 34 | 50 |
| LN24 | 262 | 265 | 376 | 33 | 60 |

## 4. Conclusions

We compared the properties of laser welds made with argon and nitrogen as shielding gases, as well as without a shielding gas.

We optimized the welding parameters and conducted a detailed analysis of the welds produced using the optimized welding parameters.

It has been found that the type of shielding gas at laser welding significantly affects the weld geometry and the heat-affected zone.

We found that the choice of shielding gas affects the hardness of the weld. As expected, argon has the least effect on hardness.

The porosity of welded joints is highest when argon is used as a shielding gas.

The tensile test revealed no differences in the measured values among the samples under consideration, as all fractures occurred in the base material.

## 4. Zaključci

Upoređena su svojstva laserski zavarenih spojeva izrađenih uz primenu argona i azota kao zaštitnih gasova, kao i bez primene zaštitnog gasa.

Optimizovani su parametri zavarivanja, nakon čega je sprovedena detaljna analiza zavarenih spojeva izrađenih primenom optimizovanih parametara.

Utvrđeno je da vrsta zaštitnog gasa pri laserskom zavarivanju značajno utiče na geometriju zavarenog spoja i zonu uticaja toplote.

Izbor zaštitnog gasa takođe utiče na tvrdoću zavarenog spoja. Očekivano, primena argona imala je najmanji uticaj na vrednosti tvrdoće.

Najveća poroznost zavarenih spojeva zabeležena je pri primeni argona kao zaštitnog gasa.

Rezultati ispitivanja zatezanjem nisu pokazali značajne razlike između razmatranih uzoraka, budući da je kod svih epruveta lom nastao u osnovnom materijalu.

**References / Literatura**

[1] D. Stanisz, T. Machniewicz, S. Parzych, G. Jeż, L. Dvorkin, and M. Hebda, Microstructure and Mechanical Properties of Joints Depending on the Process Used, Materials, vol. 15, no. 15, Aug. 2022,

doi: 10.3390/ma15155171.

[2] A. K. Sehgal, An investigation of variable welding current on impact strength of metal inert gas welded specimen, in Materials Today: Proceedings, Elsevier Ltd, 2020, pp. 3679–3682.

doi: 10.1016/j.matpr.2020.10.151.

[3] K. R. Madavi, B. F. Jogi, and G. S. Lohar, Metal inert gas (MIG) welding process: A study of effect of welding parameters, in Materials Today: Proceedings, Elsevier Ltd, 2021, pp. 690–698.

doi: 10.1016/j.matpr.2021.06.206.

[4] H. Danielewski et al., Numerical and metallurgical analysis of laser welded, sealed lap joints of s355j2 and 316l steels under different configurations, Materials, vol. 13, no. 24, pp. 1–22, Dec. 2020,

doi: 10.3390/ma13245819.

[5] E. Dogan, M. Ay, M. Kurtulmus, A. I. Yukler, and A. Etyemez, Effects of welding parameters on the angular distortion of welded steel plates, Open Chem., vol. 20, no. 1, pp. 417–423, Jan. 2022,

doi: 10.1515/chem-2022-0152.

[6] M. Suban, Determination of Stability of MIG/MAG Welding Processes, Quality and Reliability Engineering International, Vol. 17, pp. 345–353, (2001).

[7] I. Vishev, C. P. Feuring, and O. Bringmann, Implementation and evaluation of an echo state network for a quality inspection system for laser welding, in Procedia CIRP, Elsevier B.V., 2021, pp. 496–501.

doi: 10.1016/j.procir.2021.03.070.

[8] G. Casalino, S. L. Campanelli, U. D. Maso, and A. D. Ludovico, Arc leading versus laser leading in the hybrid welding of aluminium alloy using a fiber laser, in Procedia CIRP, Elsevier B.V., 2013, pp. 151–156.

doi: 10.1016/j.procir.2013.09.027.

[9] A. Sadeghian and N. Iqbal, A review on dissimilar laser welding of steel-copper, steel-aluminum, aluminum-copper, and steel-nickel for electric vehicle battery manufacturing, Feb. 01, 2022, Elsevier Ltd.

doi: 10.1016/j.optlastec.2021.107595.

[10] P. Zhang et al., A review on the effect of laser pulse shaping on the microstructure and hot cracking behavior in the welding of alloys, Aug. 01, 2021, Elsevier Ltd. doi: 10.1016/j.optlastec.2021.107094.

[11] H. Kokawa, Nitrogen absorption and desorption by steels during arc and laser welding, Welding International, vol. 18, no. 4, pp. 277–328756, 2004, doi: 10.1533/wint.2004.3235.

[12] ISO 6892-1Metallic materials-Tensile testing-Part 1: Method of test at room temperature. [Online]. Available: www.randb.co.kr,

[13] ISO 5178, 2001.